Electrohydrodynamic Inkjet Printing on Insulative Substrates with Discontinuous Gold Films

Allison Rose Tuuri

A thesis

Submitted in partial fulfillment of the

requirements for the degree of

Master of Science

University of Washington

2022

Committee:

J. Devin MacKenzie

Tanka R. Rana

Program Authorized to Offer Degree:

Materials Science and Engineering

University of Washington

Abstract

Electrohydrodynamic Inkjet Printing on Insulative Substrates with Discontinuous Gold Films

Allison Rose Tuuri

Chair of the Supervisory Committee:

J. Devin MacKenzie

Department of Materials Science and Engineering & Department of Mechanical Engineering

This study investigates process development for AC-modulated, electrohydrodynamic inkjet printing of silver nanoparticle inks on insulative surfaces. Trends were developed using printing parameters of DC bias, AC amplitude, frequency, and speed to optimize the print conditions. Print quality improved using a novel surface treatment formed by sputter coating a discontinuous gold film on insulative surfaces. Linewidths of 4 μm and single pass conductivity were achieved using the discontinuous metalized substrates.

Table of Contents

1. Introduction 1

2. Materials and Methods 3

2.1 Materials 3

2.2 Equipment 4

2.2.1 Printing 4

2.2.2 Characterization 4

2.3 Methods 4

3. Results and Discussion 8

3.1 Printing Condition Trends 8

3.1.1 DC Bias 8

3.1.2 Amplitude 9

3.1.3 Frequency 10

3.1.4 Speed 12

3.1.5 Optimization Theory 13

3.2 Discontinuous Metallic Surface Treatment 15

3.2.1 Characterization of Substrate 15

3.2.2 Print Quality 16

3.2.3 Conductivity 20

4. Conclusions 21

5. Future Work 22

Acknowledgments 23

References 24

Table of Figures

Figure 1: 5 mm x 5 mm with 100 μm linespacing printing serpentine used for parameter optimization. 6

Figure 2: a) Conductivity serpentine with 6 mm segments b) close-up of configuration serpentine 7

Figure 3: Diagram showing where the contact pads were placed and the number of print passes of each segment..... 7

Figure 4: a) Effect of decreasing DC bias on glass substrates with a 500 V amplitude, 500 Hz frequency, 50% waveform, and 3 mm/s speed. b) Effect of decreasing DC bias on PET substrates with 1000 V amplitude, 400 Hz frequency, 50% waveform, 3 mm/s speed. 9

Figure 5: a) Effect of decreasing amplitude on glass substrates with a 250 V DC bias, 500 Hz frequency, 50% waveform, and 3 mm/s speed. b) Effect of decreasing amplitude on PET substrates with a 1000 V amplitude, 400 Hz frequency, 50% waveform, 3 mm/s speed..... 10

Figure 6: a) The effects of frequency on glass substrates with a 250 V amplitude, 250 V DC bias, 50% waveform, and 3 mm/s speed. b) The effects of increasing frequency on PET substrates with an 800 V amplitude, 0 V DC bias, 50% waveform, and 3 mm/s speed..... 12

Figure 7: The effects of increasing speed on glass and PET substrates. 13

Figure 8: Graphical representation for glass and PET substrates of linewidth versus a) DC bias, b) AC amplitude, c) frequency, and d) speed. 14

Figure 9: Atomic force microscopy images of the control substrate (non-sputtered) and the experimental substrate (gold sputtered for 10s)..... 16

Figure 10: Linewidth comparison between control and experimental prints using same printing parameters with a) decreasing voltage and b) increasing frequency. 17

Figure 11: Comparison between prints made on control substrate and experimental substrate. Prints on experimental substrate show a significant decrease in feather at the edges of the traces and spray around the traces. 18

Figure 12: Images of contact angle measurements of tetradecane using elliptical fitting with 1-point tangent on a) control substrate and b) experimental substrate. 19

1. Introduction

Over the last decade, inkjet printing has become a promising fabrication method for manufacturing electronic devices, especially in the flexible electronics sector [1–3]. Current research is trying to use inkjet printing as a possible replacement for some of the photolithography processes currently used. Photolithography is a lengthy process that requires extremely clean environments. The lower the required particulate per cubic meter the cleanroom requires, the more energy intensive the operational costs are[4,5]. Inkjet printing is an additive manufacturing technique that enables rapid iteration, no-contact, digitalized fabrication with less stringent cleanliness requirements. One of the main limitations of inkjet printing is the lowest achievable resolution. Drop-on-demand (DOD) inkjet printing has individual drops printed when reservoir emits a pressure wave and ejects the ink. The two most widely used methods of drop-on-demand (DOD) inkjet are thermal and piezoelectric. Traditional DOD inkjet has a resolution limit of about 20-50 μm linewidths [6–8]. The resolution of DOD inkjet printing has many applications in flexible electronics, but the smallest achievable feature geometries are too large to replace photolithography for chip manufacturing. The resolution of traditional DOD inkjet methods is controlled by the ejected drop size. The ejected drop sizes are controlled the nozzle diameter, actuation control, and rheological properties such as surface tension, viscosity, and flow dynamics[7,9,10]. In contrast, electrohydrodynamic (EHD) inkjet printing can achieve resolution on the sub-micron scale [11,12].

Electrohydrodynamic printing manipulates the ink using an electric field to induce electric charge at the surface of the ink's meniscus. The generated surface charges within the ink cause electric stresses (Maxwell) to overcome the capillary stress. This deforms the meniscus into a

cone structure called a Taylor cone by overcoming the surface tension of the ink [13–16]. From here, two main jetting modes can occur: discontinuous and continuous jetting. Discontinuous jetting is when fragments of the ink are deposited on the substrate (like traditional drop-on-demand printing). Continuous jetting is when there is ink flowing continuously through the meniscus. The type of jetting that occurs is dependent on the strength of the electric field and the flow rate of the ink [17,18].

One of the major limitations of using EHD printing is that dielectric materials are difficult substrates to use. Since the printing method relies on an electric field potential to jet, insulative materials limit the strength of the electric field between the nozzle and the ground. One of the effects of this stack-up is that dielectric materials tend to generate more satellite formation/overspray, which limit the lowest achievable resolution[19,20]. Haque *et. al*, investigated how the electric field changes due to charge accumulation during the process. Their model confirmed that the dielectric constant of the substrate material has a considerable influence on the satellite scattering [21]. There are two approaches to minimizing satellite formation: a) tailoring ink properties, or b) modifying the printing technique. Guo *et. al* discussed that the charge relaxation time (CRT) greatly affects the droplet-meniscus repulsion. Thus, tuning the ink to meet the jetting mode is one way to reduce satellite formation [22]. Lee *et. al* overcame satellite formation by adding a ring-shaped gate electrode between the nozzle and substrate under the assumption that the electrode would help redirect and stabilize the electric field and, thus, reduce drop repulsion[23]. Tse and Barton[24] tried a different approach by having the electric field span between a positive nozzle and grounded nozzle at angles above the substrate then having airflow and an air-jetting nozzle perpendicular to the substrate. In this method, the Taylor cone is broken

due to the liquid filament being disrupted by the air flow instead of trying to use the charge to control the path[24].

In this work, EHD printing was used for micropatterning silver nanoparticle ink on two dielectric substrates, glass and polyethlylene terephthalate (PET).The goal for this research was to develop a process for printing high resolution traces on insulative substrates using a commercially available EHD printer. One method for improving trace resolution was to establish trends for the effect of different waveform parameters on print quality. The second method was to form a discontinuous, gold thin films via sputter coating on the insulative substrates.

2. Materials and Methods

2.1 Materials

The silver nanoparticle ink used in this study was AGK104 (Kishu Giken Kogyo, Co., Ltd., Japan) with a silver nanoparticle loading of 60 ± 5 wt.%, viscosity of 12 ± 3 cP at 20℃, and a surface tension of 25-30 mN/m at 20℃ in a solvent system of tetradecane[25]. The ink was filtered using 0.45 μm and 0.2 μm polytetrafluorethylene (PTFE) filters prior to nozzle loading. The substrate materials were 1 mm thick glass slides and 125 μm (5 mil) thick Melinex™ ST505 polyethylene (DuPont, USA)[26]. The experimental substrates were gold sputtered after cleaning using a 108 Manual Sputter Coater (Cressington, United Kingdom). The sputter coater was used to pull a 0.5 mbar vacuum and sputtered for 5-15s. Contact pads used a conductive silver screen printing ink, PE874 (DuPont, USA), for probing with a multimeter to measure trace resistance. Contact angle measurements were taken using DSA100 Drop Shape Analyzer (Krüss, Germany).

2.2 Equipment

2.2.1 Printing

The EHD printer was a SIJ-150 (SIJ Technologies Inc., Japan) with printing and spray coating ability. The nozzle used was a super-fine nozzle (SIJ Technologies, Inc., Japan) with a nozzle diameter between 1.3-4.5 μm[27].

2.2.2 Characterization

The trace width and thickness were measured using an LEXT OLS4100 optical profilometer (Olympus, Japan) with a fast scan speed at 50x magnification. Resistance measurements were taken using a multimeter (Fluke, USA). A Phenom ProX Desktop Scanning Electron Microscope (ThermoFisher, USA) was used for high magnification trace imaging. Substrate surface measurements were taken using a Jupiter XR Atomic Force Microscope (Oxford Instruments, United Kingdom). Contact angle measurements were taken using DSA100 Drop Shape Analyzer (Krüss, Germany).

2.3 Methods

To prepare for printing, the nozzles were filled with 10 μL of ink using a fine-tipped pipette to ensure full nozzle tip wetting and limited air gaps in the nozzle. The distance between the substrate and the nozzle was determined by bringing the nozzle tip to the surface of the substrate, then moving the nozzle up in the z-direction by 30 μm. This method was found to allow the most consistent nozzle clearance due to the variability in nozzle length and substrate thickness. The printer used five possible AC waveforms: 25%, 50%, and 75% square, sinusoidal, and triangular. All substrates were cleaned with 2 vol.% detergent and deionized water, isopropyl alcohol, and acetone and dried using compressed nitrogen (N_2) between each step. The glass slides were surface treated via UV-Ozone for 10 minutes. The untreated, cleaned substrates will thus be

referred to as the “control substrates”. The “experimental substrates” were sputtered with gold for 10 s after cleaning. The sputter time was determined by testing sputter times in increments of 5 s with 10 s determined to be the greatest improvement of print quality without forming a conductive surface. The printing parameters evaluated were waveform, amplitude [V], DC bias [V], speed [mm/s], and frequency [Hz].

All permutations of print parameters were printed on both the control and experimental substrates on the same day. The control print conditions were based off the recommendations from the EHD printer manufacturer (SIJ Technologies) and are described in Table I. Before each printing session, the control parameters were printed on each substrate to ensure the nozzle was not clogged and the printer was working properly. The control conditions for glass and PET substrates are different because the minimum conditions for jetting vary from substrate to substrate.

Table I: Control Print Conditions for AGK104

Variable	**Glass Conditions**	**PET Conditions**
DC Bias [V]	500	0
Amplitude [V]	500	500
Frequency [Hz]	500	200
Speed [mm/s]	3	3
Waveform	50% Square	50% Square

The printing pattern used was a 5 mm x 5 mm serpentine with 100 μm line spacing (Figure 1). Each permutation was printed for 10 lines of the pattern before the variable was changed. Before the beginning of each print, the nozzle had a “spit” voltage applied to ensure proper ink flow to the tip of the nozzle. The spit voltage trended upwards over the length of printing due to the aggregation of nanoparticles at the tip over time.

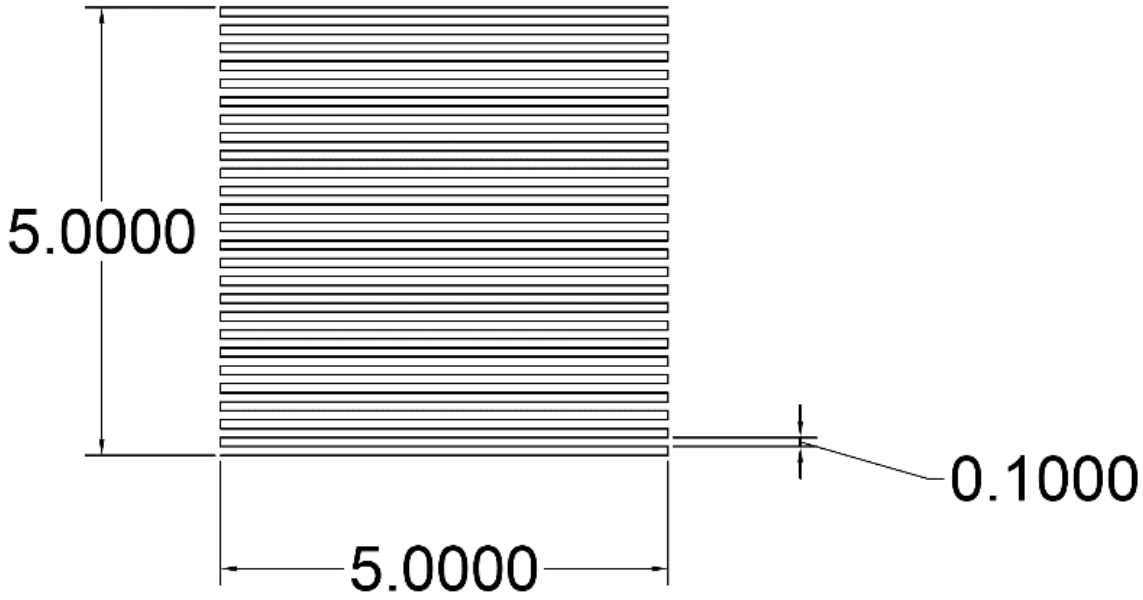

Figure 1: 5 mm x 5 mm with 100 μm linespacing printing serpentine used for parameter optimization.

A 6 mm x 6 mm serpentine trace was designed to understand whether the discontinuous film influences the conductivity (Figure 2a). In this design, there are twenty lines with 100 μm spacing prior to the measurable traces to allow for parameter configuration (Figure 2b). Silver screen printing paste was applied on the vertices of the 6 mm x 6 mm portion of the serpentine to function as contact pads for measuring resistance (gray contact points in Figure 3). Each horizontal 6 mm segment had resistance measured after sintering the traces and curing the contact pads. The serpentine was divided into five sets of two segments. Each set of two segments had a different number of passes starting from the top two segments having a single pass to the bottom two traces having five passes (Figure 3).

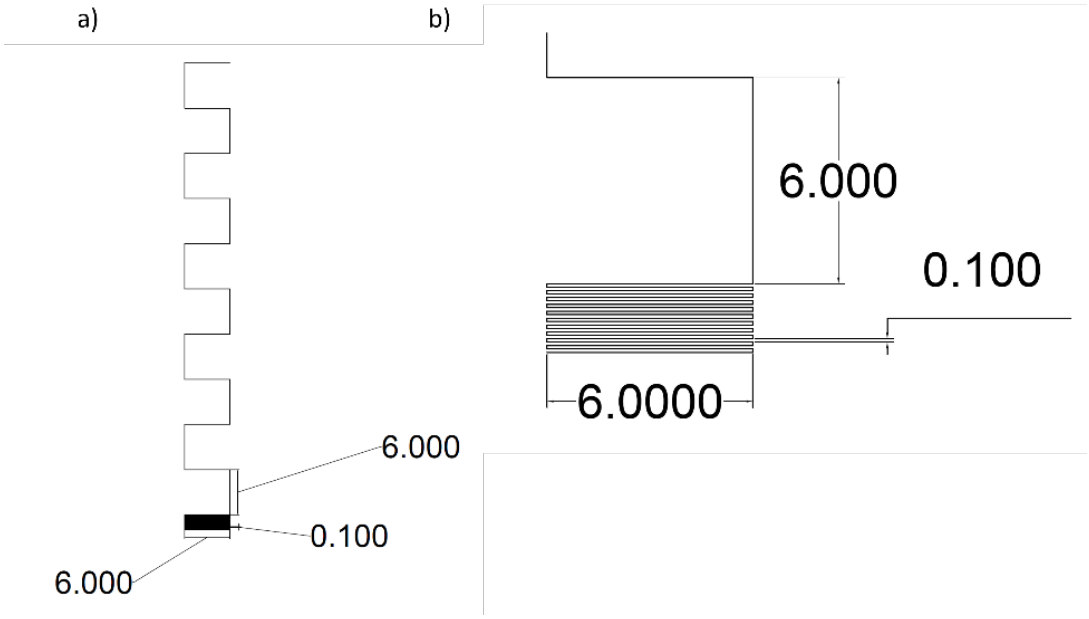

Figure 2: a) Conductivity serpentine with 6 mm segments b) close-up of configuration serpentine

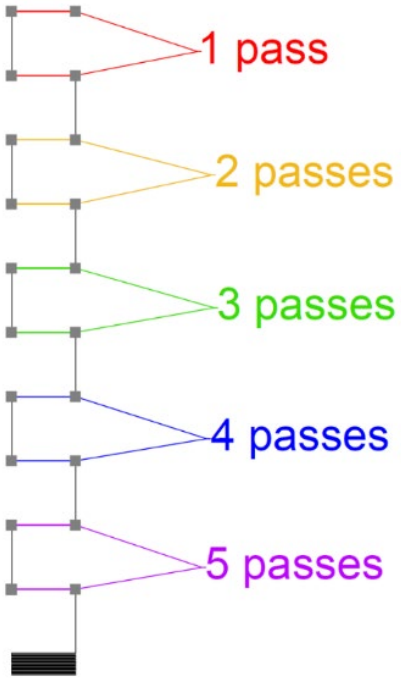

Figure 3: Diagram showing where the contact pads were placed and the number of print passes of each segment.

3. Results and Discussion

3.1 Printing Condition Trends

By changing the value of different printing conditions, trends in print quality and linewidth were observed. With every setting, there is a point at which the printer can no longer produce a continuous line, whether it stops jetting or becomes individual dots due to insufficient electric field. To observe the effect of each condition, a variable was changed in an incremental value until parameter produces thin, uniform trace. That value was used as the base value for the next variable. The following trends were consistent between substrate materials and between the control and experimental conditions.

3.1.1 DC Bias

The DC bias is the applied DC voltage that shifts the AC waveform either up or down. The DC bias changes the crest and trough voltages but does not change the amplitude or frequency of the waveform. Applying a DC bias makes both the peak of the waveform and the trough of the waveform higher, increasing the overall potential applied. As the DC bias decreased with the glass substrates, the linewidths decreased by approximately 50% with each 100 V decrease (Figure 4a). The prints became discontinuous at 200 V and stopped jetting at 100 V. The decrease of linewidth until discontinuity was caused by a decrease in the strength of the electric field. Starting from the control, the 50% waveform has a maximum applied voltage of 1000 V and a minimum of 0 V. As that bias is shifted down, the total potential decreases and makes it more difficult to overcome the insulator.

Altering the DC bias on PET causes two trends to occur. The same decrease in linewidth occurs as with the glass substrate, however, the PET substrates also display a decrease in overspray at the edges of the traces (Figure 4b). Wei *et al.*[28] showed in a 2014 study that using AC-pulse

modulation without a DC bias contribution, the ejected droplets have alternating charges of equal magnitude based on the amplitude of the wave. In turn, the charge imparted to the substrate surface is neutralized between adjacent drops, which eliminates charge accumulation. With a DC bias, the alternating charge magnitudes are unequal, which suggests incomplete neutralization of the imparted surface charges. For the glass substrates, DC bias is required for the electric field to overcome the increased capacitance attributed to from the thicker substrate and higher dielectric constant.

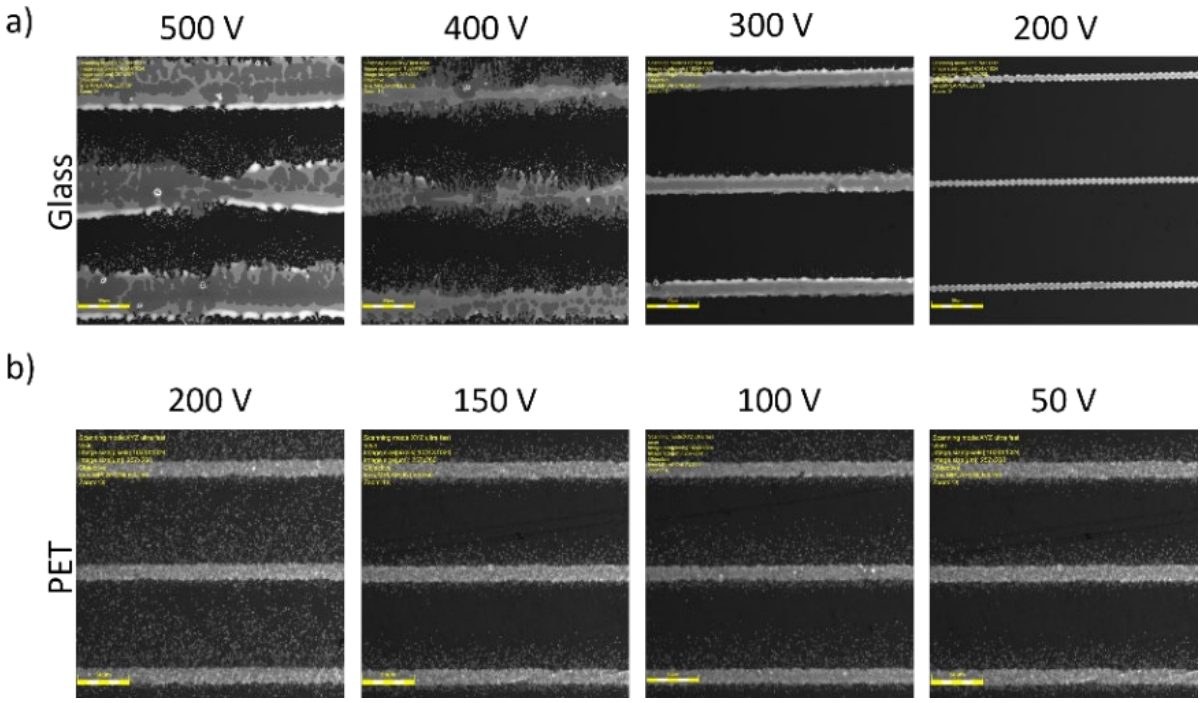

Figure 4: a) Effect of decreasing DC bias on glass substrates with a 500 V amplitude, 500 Hz frequency, 50% waveform, and 3 mm/s speed. b) Effect of decreasing DC bias on PET substrates with 1000 V amplitude, 400 Hz frequency, 50% waveform, 3 mm/s speed.

3.1.2 Amplitude

The amplitude is the difference between the peak/trough of the wave and the centerline. Much like the DC bias, the amplitude changes the potential of the electric field by switching the

polarity of the electric field. Decreasing the amplitude of the AC current decreases the linewidth for both glass and PET substrates (Figure 5). High amplitudes formed trace widths higher than the pitch of the serpentine. Larger amplitudes cause stronger electric fields, which causes more deposition of ink. For glass substrates, a DC bias must be applied at any amplitude. For PET substrates, there is a range of higher amplitudes that can form jets without a DC bias. Adjusting the DC bias impacts which amplitudes allow for stable jetting. The traces on glass substrates had less overspray compared to the PET substrates, indicating that glass and PET have different charge dissipation rates.

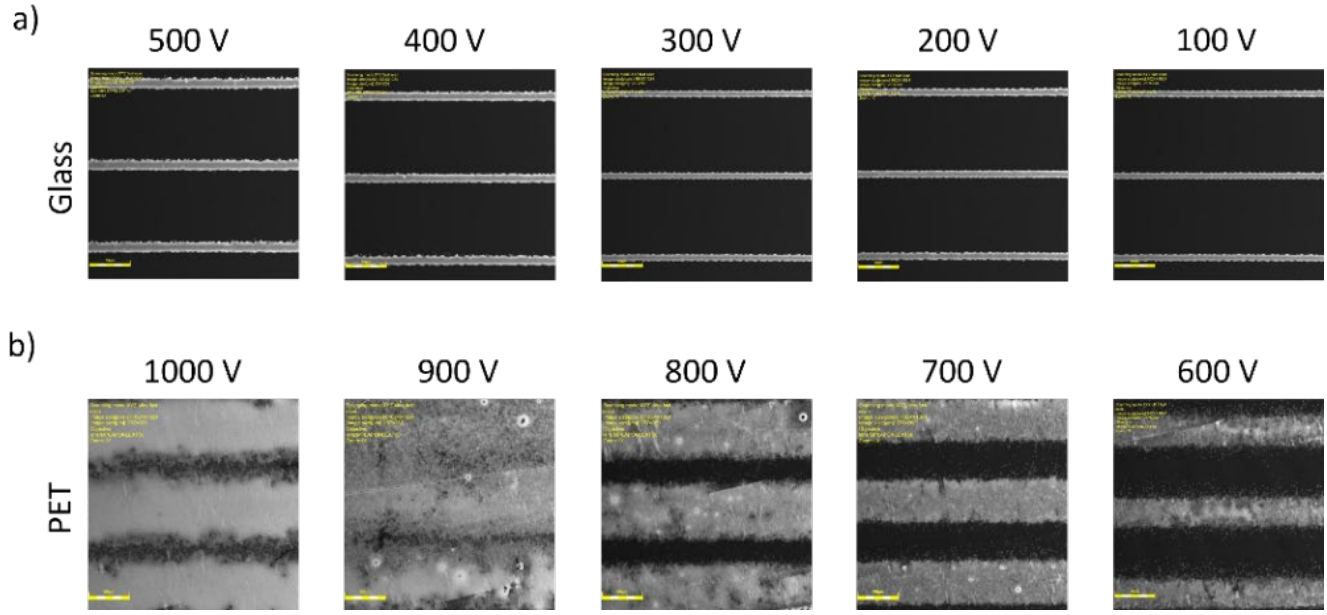

Figure 5: a) Effect of decreasing amplitude on glass substrates with a 250 V DC bias, 500 Hz frequency, 50% waveform, and 3 mm/s speed. b) Effect of decreasing amplitude on PET substrates with a 1000 V amplitude, 400 Hz frequency, 50% waveform, 3 mm/s speed.

3.1.3 Frequency

The frequency is the number of cycles that occur in a period. In the context of EHD inkjet, the frequency is how often the ink jets from the nozzle. For both glass and PET substrates, increasing the frequency decreases the linewidth (Figure 6). The increasing frequency of jetting

causes the Taylor cone to form for shorter periods of time. This causes smaller droplets to be dispensed because there is less time for the droplet to be formed at the tip of the meniscus. Frequency was the most impactful parameter on linewidth because an incremental change in frequency changed the linewidth more dramatically than voltage. There are frequency ranges that allow jetting between the two substrates. For glass, the upper limit is ~900 Hz while the upper limit for PET is ~450 Hz. An explanation for the difference in achievable maximum frequency is the nature of the Taylor cone and how it induces jetting. When printing using AC waveforms without DC bias, the Taylor cone is possibly forming only at the peaks and troughs of the waveform and completely dissipating when moving through the nodes. In contrast, applying a DC bias, the Taylor cone is continuously present (cone-jet mode), and the AC amplitude is modulating the meniscus. The upper limit changes with the overall potential of the waveform. The higher the potential, the higher frequencies cause jetting. For line optimization, the highest frequency available for the substrate should be used with the most stable jetting cone formed by adjust the DC bias and amplitude.

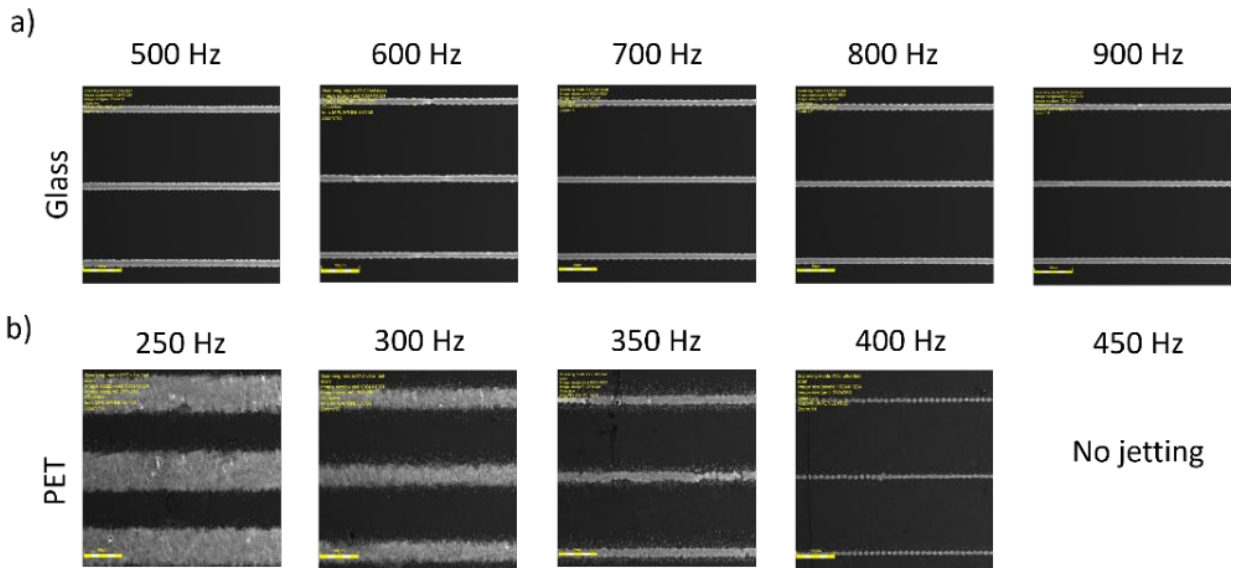

Figure 6: a) The effects of frequency on glass substrates with a 250 V amplitude, 250 V DC bias, 50% waveform, and 3 mm/s speed. b) The effects of increasing frequency on PET substrates with an 800 V amplitude, 0 V DC bias, 50% waveform, and 3 mm/s speed.

3.1.4 Speed

The speed is how fast the nozzle head moves across the printing surface. In general, the faster the nozzle moves, the thinner the linewidth due to an increase in drop spacing. Eventually, the nozzle is moving too fast to form a continuous line (Figure 7). The effects of the speed on linewidth are not necessarily substrate dependent. The stability of jetting at a given amplitude, bias, and frequency are all ink-substrate dependent. For both substrates, the upper limit for speed is 4 mm/s, but the best continuity speed is at 3 mm/s after optimizing for other variables. Higher speeds could be used for more stable jetting parameters but will not have a significant impact on reducing linewidth.

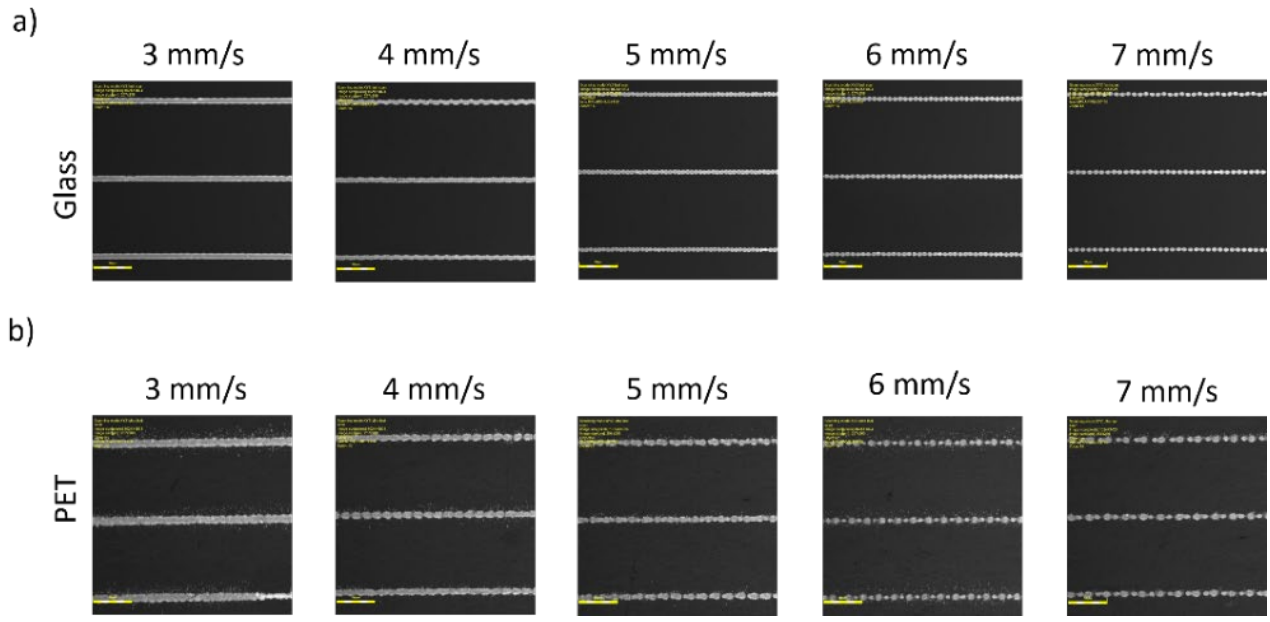

Figure 7: The effects of increasing speed on glass and PET substrates.

3.1.5 Optimization Theory

The quality of print achievable using EHD printing is dependent on the substrate and ink used. Since EHD printing is dependent on the magnitude of the electric field between the nozzle and the ground plane, the conductivity of the substrate and conductivity of the ink used can affect the parameters used. The overall trends found were a) linewidth deceases with decreasing DC bias for glass substrates, and overall reduces spray on PET substrates, b) decreasing AC amplitude decreases linewidth for both substrates, c) increasing frequency decreases linewidth for both substrates, and d) increasing speed decreases linewidth for both substrates (Figure 8).

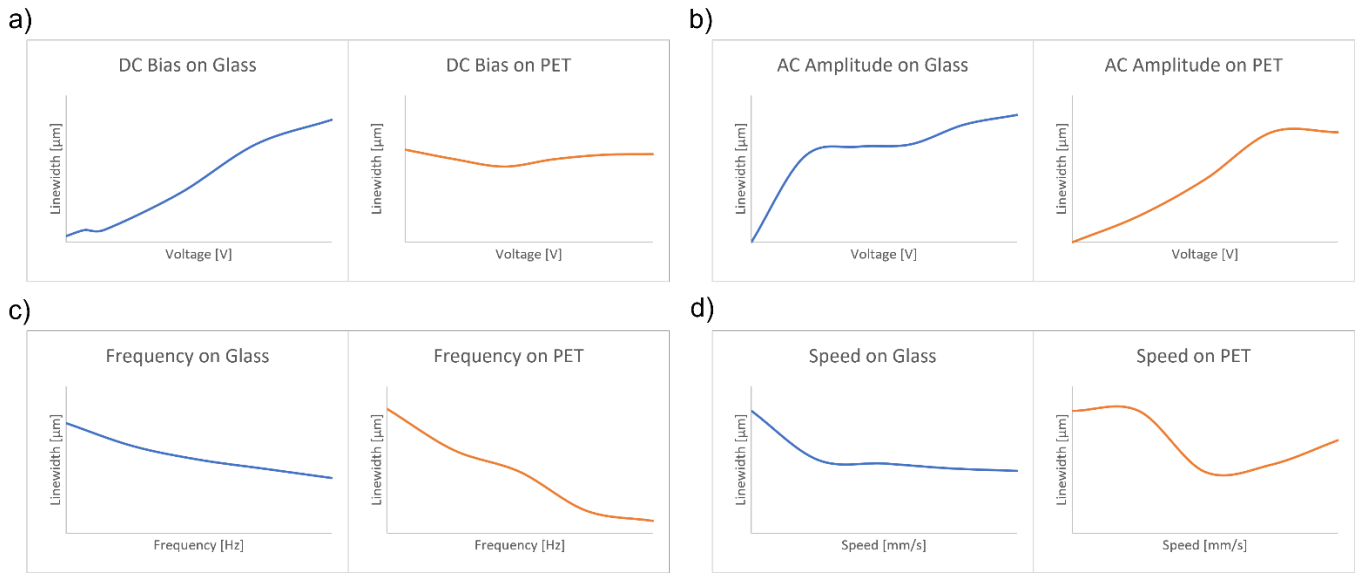

Figure 8: Graphical representation for glass and PET substrates of linewidth versus a) DC bias, b) AC amplitude, c) frequency, and d) speed.

Using the trends described above, the method for determining the optimal printing parameters of silver nanoparticle inks should be follow these basic tenants:

1. Use the highest frequency possible.
2. Use the highest possible speed that forms continuous lines without breakup.
3. Alter the DC bias and amplitude of the waveform to achieve the best line quality without diminishing jetting following the basic principle of the lower the voltage, the thinner the linewidth.

One of the limitations for this printing process is that the printing parameters do not stay consistent from print to print. How recently the ink was filtered, difference in substrate roughness, changes in humidity, and nozzle clearance all can impact the voltages and frequencies that can be used. Where the process is now, the printing parameters need to be configured for each print set-up and substrate.

3.2 Discontinuous Metallic Surface Treatment

3.2.1 Characterization of Substrate

The surface of the substrates after sputtering were investigated to determine whether the gold made the surface conductive. A dielectric substrate is preferred for device fabrication for many device applications to prevent shorting between printed features. Scanning electron microscopy was used to better understand the topology of the film. During imaging, the metallic film was not able to eliminate charging, indicating the film was discontinuous. To determine whether the discontinuous metallic film would cause shorting between traces, interdigitated electrodes (IDEs) were printed on both the gold sputtered glass and PET substrates. The IDE structures had 20 fingers with a 15 μm pitch. The inks were sintered, and silver paste was applied and cured on the contact pads. None of the IDEs were conductive between the two segments at room temperature, indicating the surface treatment would not short devices printed using this method.

Atomic force microscopy was used to determine whether gold sputtering roughness of the substrate changes after deposition. Two samples were characterized, one control glass substrate and one experimental substate. Since EHD printing is dependent on the clearance between the nozzle and substrate, changes in roughness could impact the printing process. The box size used was 1 μm^2 with 500 nm offsets. A visual comparison between the control and experimental shows that the experimental substrate has a more uniform roughness on the surface compared to the control sample (Figure 9).

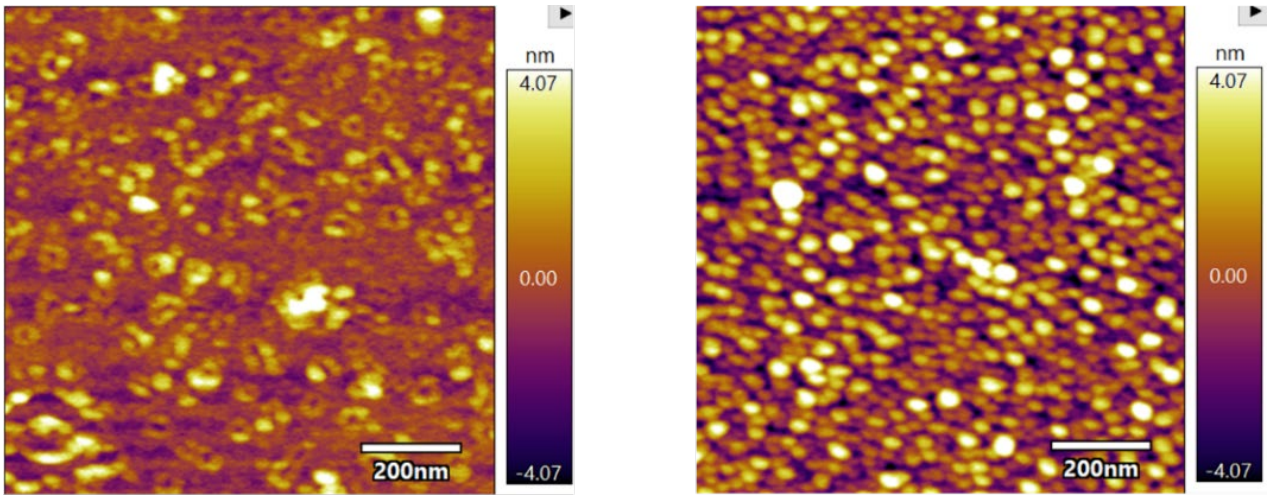

Control Glass

Experimental Glass

Figure 9: Atomic force microscopy images of the control substrate (non-sputtered) and the experimental substrate (gold sputtered for 10s).

3.2.2 Print Quality

When the prints on the experimental substrates are compared to the control prints of the same settings, there are substantial improvements on the quality of the traces using the same parameters. The experimental prints tend had an overall reduction in linewidth, less "spray", and less feathering of the traces. The average linewidth reduction for the experimental substrates compared to the control substrates using the same settings was 45.5± 0.3% (Figure 10). Average percent change was calculated by taking the mean linewidth for each permutation and finding the percent change between those two means. The mean of the percent changes was calculated. The standard error of mean was calculated using the sample standard deviation.

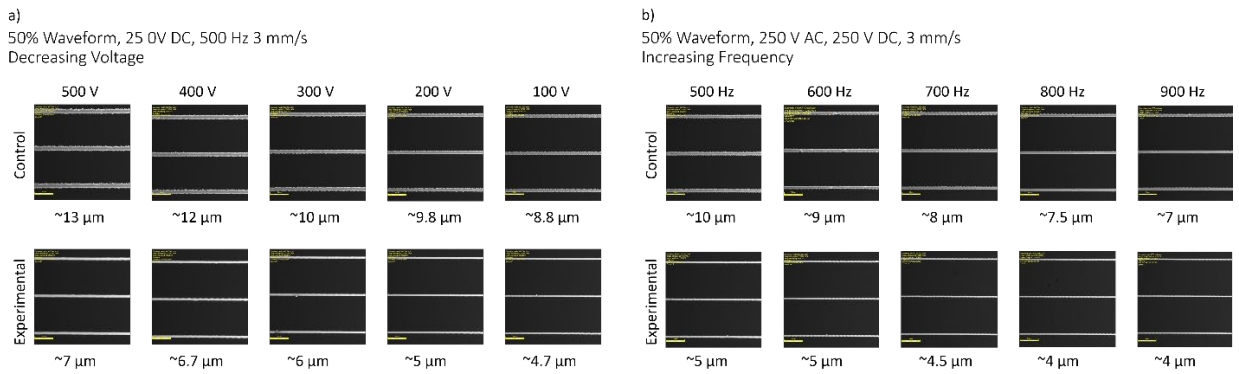

Figure 10: Linewidth comparison between control and experimental prints using same printing parameters with a) decreasing voltage and b) increasing frequency.

The experimental substrate also improved the trace resolution and precision (Figure 10). With the control substrates, the edges of the traces tend to have a "feathering" effect, where the ink spreads away from the initial trace onto the substrate before drying. The wider control prints also tend to experience more overspray from satellite formation. The experimental prints have tighter trace edges and a substantial reduction in overspray, which improves the achievable resolution of the prints (**Figure 11**).

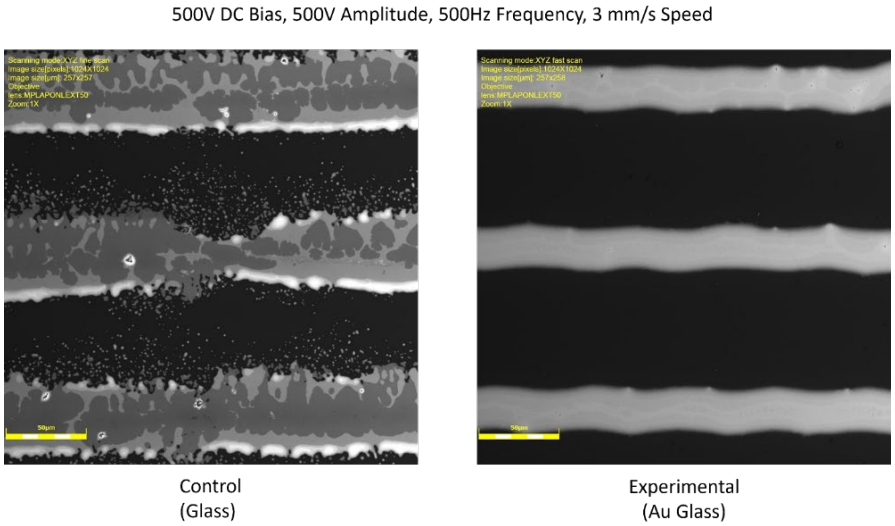

Figure 11: Comparison between prints made on control substrate and experimental substrate. Prints on experimental substrate show a significant decrease in feather at the edges of the traces and spray around the traces.

It is well established that surface energy plays a significant role in EHD printing [29,30]. To understand whether the discontinuous gold film changed the surface energy of the substrate to improve ink wetting (and thus improved print quality), contact angle measurements were taken of both tetradecane and AGK104 using the sessile drop type and ellipse 1-point tangent fitting method. From contact angle measurements, the surface free energy (SFE) was calculated using the Owens, Wendt, Rabel and Kaelble (OWRK) method[31]. The mean contact angle of tetradecane on the control substrate was 21.23° with a standard deviation of 2.56° (Figure 12a). The mean contact angle of tetradecane on the experimental substrate was 12.86° with a standard deviation of 2.89° (Figure 12b). However, when the SFE is calculated, the control substrate was 66.37 mN/m with a standard deviation of 2.29 mN/m, and the experimental substrate was 67.65 mN/m with a standard deviation of 2.6 mN/m. The percent change of SFE was a 1.9% increase under the experimental condition, which does not indicate the gold film greatly alters the wettability of the substrate. The AGK104 experienced total wetting on all substrate conditions

and prevented the SFE from being modeled. Because of the insignificant change in SFE using tetradecane and the total wetting of AGK104, it can be concluded that the improvement in print quality was not due to changes in the surface energy due to the gold discontinuous film.

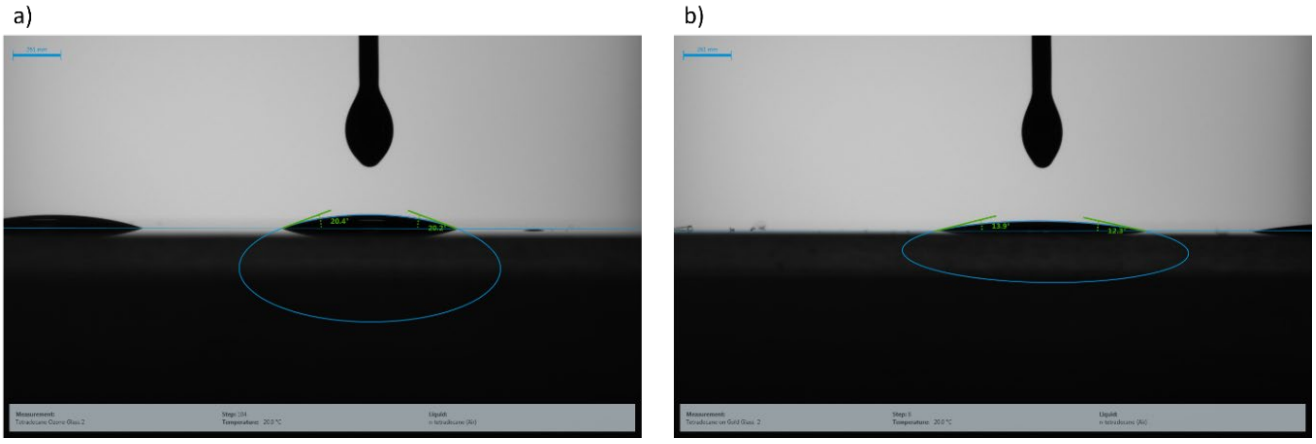

Figure 12: Images of contact angle measurements of tetradecane using elliptical fitting with 1-point tangent on a) control substrate and b) experimental substrate.

An explanation as to why print quality improves with the additional experimental treatment is that the gold helps dissipate the surface charge that has accumulated on the dielectric substrates. Since the formation of the Taylor cone occurs due to charge being induced on the surface of the ink, the ink carries a polarity. This has three effects on the printing process: a) the electric field is constantly changing due to charged particles disrupting the field [21,32], b) the droplets can repel each other due to like-charges and cause spray [33,34], and c) the charged droplets cause retained surface charges on the substrate. Additionally, since the substrates are being exposed to an electric field for a prolonged period, the surface of the substrate accumulates residual charge [35]. In substrates like PET, that charge can be retained for weeks after printing dependent on environmental conditions such as temperature, humidity, and the initial charge density [36]. Though the metalized surface is discontinuous, the gold absorbs the retained charge instead of the insulative substrate and allows the charge to percolate away from the jet. The suspected mode

of charge dissipation is a tunneling conduction mechanism through the assumed "islands" of the gold film. Electron tunneling between gold nanoparticles separated by insulators has been well studied[37–40]. For this application, it is premised the tunneling effect is great enough to allow the charge to move away from the localized electric field allowing for jetting, but not strong enough to be measurably conductive. Dissipation of excess charge reduces the satellite drop repulsion, thus reducing overspray. The regularity of the Taylor cone also improves since the electric field is more stable.

3.2.3 Conductivity

The traces on the experimental substrates had superior conductance compared to the control prints. The control substrates only had measurable resistance on two of the five pass traces. Conversely, the traces on the experimental substrates had measurable resistances for single passes. When the five pass traces were compared, the average resistance of the experimental traces was 39% lower than the control condition. Using the resistance, film thickness, linewidth, and length, the resistivity was calculated and averaged (Table II). The resistivity of the experimental traces was not consistent between the different number of passes. The average resistivity was $2.09 \times 10^{-5} \pm 4.97 \times 10^{-6}$ Ω-cm. The spread of resistivities did not have a trend, preventing any conclusions to be drawn from this dataset. Trends were also not drawn between substrate conditions since the control substrates did not have measurable conductivity. An explanation to why the experimental condition allowed for single pass conductivity due to the gold islands sintering with the silver nanoparticles in the ink. Since inks developed for inkjet require a controlled viscosity and surface tension range, the particle loading of most inks is relatively low. By introducing a small amount of gold, the silver nanoparticles were able to sinter

more continuously than on a bare substrate. This reduces the cracks in the trace, thus improving electron flow.

Table II: Calculated Resistivities for Different Number of Passes

Passes	**Control [Ω-cm]**	**Experimental [Ω-cm]**
5	1.63×10^{-5} (n=2)	1.11×10^{-5} (n=5)
4	Open	9.33×10^{-6} (n=4)
3	Open	1.05×10^{-5} (n=4)
2	Open	8.41×10^{-6} (n=5)
1	Open	6.54×10^{-5} (n=2)

4. Conclusions

Through this work, trends were established for how different waveform parameters have an effect on the print quality of silver nanoparticle inks on insulative substrates using EHD inkjet printing on a SIJ-150 commercial system. Increasing the frequency and decreasing the amplitude of the waveform causes a reduction in linewidth. Decreasing the DC bias reduces the amount of overspray and the linewidth. Increasing the speed is insignificant compared to other parameters to reducing linewidth. The DC bias and amplitude stabilizes the jet, while the frequency changes the linewidth based on that stability. For optimization, the frequency should be maximized, while the DC bias and amplitude are balanced to match that frequency and produce the finest linewidth.

The use of discontinuous metallic films has a promising effect to further improve the resolution of EHD printing. Using a discontinuous metalized film on an insulating substrate dissipates the surface charge caused by the printing process. By eliminating the retained charge, the electric field stabilizes, reducing satellite scattering and improving the stability of the Taylor cone to allow for improved jetting. The elimination of stray charges also allows for lower electric fields to be used, resulting in narrower linewidths and greater precision. This improvement in print

quality and the possibility of single pass conductivity are promising indicators that this concept is viable.

5. Future Work

Further optimization for printing on insulators with discontinuous, metallic films is needed to better understand the mechanism and stabilize the process. The nature of the films needs further characterization as well. Measuring the corona charge decay rate of insulators with discontinuous gold films would support the charge-dissipation hypothesis. Low vacuum SEM imaging at a higher magnification would be useful to better understand the morphology of the film. Understanding the particle size of the gold film would help support the hypothesis of electric tunneling across the surface to dissipate charge.

Exploring metals other than gold would help understand the characteristics required to allow this phenomenon to occur. Using different metals/alloys also introduces other variables, such as oxidation, alloying effects with the inks, and possible degradation over time.

Conductive polymers should also be considered as replacements for metallic films. Continuous films of conductive polymers could also be used and then be surface treated to make the surface dielectric. Exploring conductive polymers would also be beneficial to understand the conductivity requirements and limitations of the film to improve the printing process. Potential applications include composite, transparent electrodes composed of EHD inkjet-printed silver grids on weakly conducting, transparent conductive polymers.

Acknowledgments

First, thank you to Prof. J. Devin MacKenzie for the opportunity to do this work. His input and opinions helped me think of problems from a different angle. All the thanks and appreciation to Michael Crump for his guidance, advice, emotional support on this project and for continuing the research. Thank you to Dr. Phillip Cox for characterization assistance and the whole Washington Clean Energy Testbeds staff for training, advice, and support. Lastly, thanks to the SPEED group for always being helping work brainstorm different solutions and giving me people to talk to in the lab.

References

(1) Tobjörk, D.; Kaihovirta, N. J.; Mäkelä, T.; Pettersson, F. S.; Österbacka, R. All-Printed Low-Voltage Organic Transistors. *Organic Electronics* **2008**, *9* (6), 931–935. https://doi.org/10.1016/j.orgel.2008.06.016.

(2) Aernouts, T.; Aleksandrov, T.; Girotto, C.; Genoe, J.; Poortmans, J. Polymer Based Organic Solar Cells Using Ink-Jet Printed Active Layers. *Applied Physics Letters* **2008**, *92* (3), 33306. https://doi.org/10.1063/1.2833185.

(3) Kuil, M. E.; Abrahams, J. P.; Marijnissen, J. C. M. Nano-Dispensing by Electrospray for Biotechnology. *Biotechnology Journal* **2006**, *1* (9), 969–975. https://doi.org/10.1002/biot.200600062.

(4) Zajic, I.; Larkowski, T.; Hill, D.; Burnham, K. J. Temperature Model of Clean Room Manufacturing Area for Control Analysis; Stevenage, UK: IET: Stevenage, UK, 2010; pp 1251–1256. https://doi.org/10.1049/ic.2010.0460.

(5) Xu, T. Characterization of Minienvironments in a Clean Room: Design Characteristics and Environmental Performance. *Building and Environment* **2007**, *42* (8), 2993–3000. https://doi.org/10.1016/j.buildenv.2006.10.020.

(6) Szczech, J. B.; Megaridis, C. M.; Gamota, D. R.; Zhang, J. Fine-Line Conductor Manufacturing Using Drop-on Demand PZT Printing Technology. *IEEE transactions on electronics packaging manufacturing* **2002**, *25* (1), 26–33. https://doi.org/10.1109/TEPM.2002.1000480.

(7) Derby, B. Inkjet Printing of Functional and Structural Materials: Fluid Property Requirements, Feature Stability, and Resolution. *Annual Review of Materials Research* **2010**, *40* (1), 395–414. https://doi.org/10.1146/annurev-matsci-070909-104502.

(8) Lemarchand, J.; Bridonneau, N.; Battaglini, N.; Carn, F.; Mattana, G.; Piro, B.; Zrig, S.; Noël, V. Challenges, Prospects, and Emerging Applications of Inkjet-Printed Electronics: A Chemist's Point of View. *Angewandte Chemie International Edition* **2022**, *61* (20), e202200166-n/a. https://doi.org/10.1002/anie.202200166.

(9) Nayak, L.; Mohanty, S.; Kumar Nayak, S.; Ramadoss, A. A Review on Inkjet Printing of Nanoparticle Inks for Flexible Electronics. *J. Mater. Chem. C* **2019**, *7* (29), 8771–8795. https://doi.org/10.1039/c9tc01630a.

(10) Dong, H.; Carr, W. W.; Morris, J. F. An Experimental Study of Drop-on-Demand Drop Formation. *Physics of Fluids* **2006**, *18* (7), 072102-072102–072116. https://doi.org/10.1063/1.2217929.

(11) Park, J. U.; Hardy, M.; Kang, S. J.; Barton, K.; Adair, K.; Mukhopadhyay, D. K.; Lee, C. Y.; Strano, M. S.; Alleyne, A. G.; Georgiadis, J. G.; Ferreira, P. M.; Rogers, J. A.; Jun Kang, S.; Barton, K.; Adair, K.; Kishore Mukhopadhyay, D.; Young Lee, C.; Strano, M. S.; Alleyne, A. G.; Georgiadis, J. G.; Ferreira, P. M.; Rogers, J. A. High-Resolution Electrohydrodynamic Jet Printing. *Nature Materials* **2007**, *6* (10), 782–789. https://doi.org/10.1038/nmat1974.

(12) Poon, H. F. Electrohydrodynamic Printing, Princeton University, Princeton, NJ, 2002.

(13) Byun, D.; Lee, Y.; Tran, S. B. Q.; Nugyen, V. D.; Kim, S.; Park, B.; Lee, S.; Inamdar, N.; Bau, H. H. Electrospray on Superhydrophobic Nozzles Treated with Argon and Oxygen Plasma. *Applied Physics Letters* **2008**, *92* (9), 93507. https://doi.org/10.1063/1.2840725.

(14) Yudistira, H. T.; Nguyen, V. D.; Dutta, P.; Byun, D. Flight Behavior of Charged Droplets in Electrohydrodynamic Inkjet Printing. *Applied Physics Letters* **2010**, *96* (2), 023503-023503–3. https://doi.org/10.1063/1.3280077.

(15) Tse, L.; Barton, K. A Field Shaping Printhead for High-Resolution Electrohydrodynamic Jet Printing onto Non-Conductive and Uneven Surfaces. *Applied Physics Letters* **2014**, *104* (14), 143510. https://doi.org/10.1063/1.4871103.

(16) Phung, T. H.; Oh, S.; Kwon, K. S. High-Resolution Patterning Using Two Modes of Electrohydrodynamic Jet: Drop on Demand and Near-Field Electrospinning. *Journal of Visualized Experiments : JoVE* **2018**, No. 137, 57846. https://doi.org/10.3791/57846.

(17) Jaworek, A.; Krupa, A. Classification of the Modes of EHD Spraying. *Journal of Aerosol Science* **1999**, *30* (7), 873–893. https://doi.org/10.1016/S0021-8502(98)00787-3.

(18) Park, J.-U.; Lee, S.; Unarunotai, S.; Sun, Y.; Dunham, S.; Song, T.; Ferreira, P. M.; Alleyene, A. G.; Paik, U.; Rogers, J. A. Nanoscale, Electrified Liquid Jets for High-Resolution Printing of Charge. *Nano Letters* **2010**, *10* (2), 584–591. https://doi.org/10.1021/nl903495f.

(19) Huo, Y.; Wang, J.; Zuo, Z.; Fan, Y. Visualization of the Evolution of Charged Droplet Formation and Jet Transition in Electrostatic Atomization. *Physics of fluids (1994)* **2015**, *27* (11), 114105. https://doi.org/10.1063/1.4935881.

(20) Son, S.; Lee, S.; Choi, J. Fine Metal Line Patterning on Hydrophilic Non-Conductive Substrates Based on Electrohydrodynamic Printing and Laser Sintering. *Journal of Electrostatics* **2014**, *72* (1), 70–75. https://doi.org/10.1016/j.elstat.2013.12.002.

(21) Haque, S.; Lee, S.; Son, S. Effect of Charge Accumulation and Dielectric Polarization on EHD Patterning on Non-Conductive Substrates. In *Advanced Manufacturing, Electronics and Microsystems: TechConnect Briefs 2015*; Washington, 2015; Vol. 4, pp 396–399.

(22) Guo, L.; Duan, Y.; Deng, W.; Guan, Y.; Huang, Y. A.; Yin, Z. Charged Satellite Drop Avoidance in Electrohydrodynamic Dripping. *Micromachines (Basel)* **2019**, *10* (3), 172. https://doi.org/10.3390/mi10030172.

(23) Lee, S.; An, K.; Son, S.; Choi, J. Satellite/Spray Suppression in Electrohydrodynamic Printing with a Gated Head. *Applied Physics Letters* **2013**, *103* (13), 133506. https://doi.org/10.1063/1.4822264.

(24) Tse, L.; Barton, K. Airflow Assisted Printhead for High-Resolution Electrohydrodynamic Jet Printing onto Non-Conductive and Tilted Surfaces. *Applied Physics Letters* **2015**, *107* (5), 054103. https://doi.org/10.1063/1.4928482.

(25) Kishu Giken Kogyo Co. Ltd. *KGK Nano AGK 103, 104*. https://www.kishugiken.co.jp/nanoweb/lineup.html (accessed 2022-05-02).

(26) DuPont. MELINEX® ST505 Product Description Approvals Typical Properties. 2005.

(27) Shimizu, K. Inquiry from SIJ Contact. September 13, 2021.

(28) Wei, C.; Qin, H.; Ramírez-Iglesias, N. A.; Chiu, C. P.; Lee, Y. S.; Dong, J. High-Resolution Ac-Pulse Modulated Electrohydrodynamic Jet Printing on Highly Insulating Substrates. *Journal of Micromechanics and Microengineering* **2014**, *24* (4), 45010–45019. https://doi.org/10.1088/0960-1317/24/4/045010.

(29) Jin Jeong, Y.; Lee, H.; Lee, B.-S.; Park, S.; Teguh Yudistira, H.; Choong, C.-L.; Park, J.-J.; Eon Park, C.; Byun, D. Directly Drawn Poly(3-Hexylthiophene) Field-Effect Transistors by Electrohydrodynamic Jet Printing: Improving Performance with Surface Modification. *ACS Applied Materials and Interfaces* **2014**, *6* (13), 10736–10743. https://doi.org/10.1021/am502595a.

(30) Kwon, J.; Hong, S.; Suh, Y. D.; Yeo, J.; So, H.-M.; Chang, W. S.; Ko, S. H. Direct Micro Metal Patterning on Plastic Substrates by Electrohydrodynamic Jet Printing for Flexible Electronic Applications. *ECS Journal of Solid State Science and Technology* **2015**, *4* (4), P3052–P3056. https://doi.org/10.1149/2.0081504JSS.

(31) Owens, D. K.; Wendt, R. C. Estimation of the Surface Free Energy of Polymers. *J Appl Polym Sci* **1969**, *13* (8), 1741–1747. https://doi.org/10.1002/app.1969.070130815.

(32) Tang, K.; Gomez, A. On the Structure of an Electrostatic Spray of Monodisperse Droplets. *Physics of fluids (1994)* **1994**, *6* (7), 2317–2332. https://doi.org/10.1063/1.868182.

(33) Nguyen, V. D.; Byun, D. Mechanism of Electrohydrodynamic Printing Based on Ac Voltage without a Nozzle Electrode. *Appl Phys Lett* **2009**, *94* (17), 173509. https://doi.org/10.1063/1.3126957.

(34) Kim, B.; Kim, I.; Joo, S. W.; Lim, G. Electrohydrodynamic Repulsion of Droplets Falling on an Insulating Substrate in an Electric Field. *Appl. Phys. Lett* **2009**, *95*, 204106-204106–3. https://doi.org/10.1063/1.3262946.

(35) le Gressus, C.; Valin, F.; Gautier, M.; Duraud, J. P.; Cazaux, J.; Okuzumi, H. Mechanisms and Applications: Charging Phenomena in Insulating Materials. *Scanning* **1990**, *12* (4), 203–210. https://doi.org/10.1002/sca.4950120406.

(36) Herous, L.; Remadnia, M.; Kachi, M.; Nemamcha, M. Decay of Electrical Charges on Polyethylene Terephthalate Surface Engineering Science and Technology Review. *Journal of Engineering Science and Technology Review* **2009**, *2* (1), 87–90. https://doi.org/10.25103/jestr.021.17.

(37) Simmons, J. G. Generalized Formula for the Electric Tunnel Effect between Similar Electrodes Separated by a Thin Insulating Film. *Journal of Applied Physics* **1963**, *34* (6), 1793. https://doi.org/10.1063/1.1702682.

(38) Zamborini, F. P.; Leopold, M. C.; Hicks, J. F.; Kulesza, P. J.; Malik, M. A.; Murray, R. W. Electron Hopping Conductivity and Vapor Sensing Properties of Flexible Network Polymer Films of Metal Nanoparticles. *J Am Chem Soc* **2002**, *124* (30), 8958–8964. https://doi.org/10.1021/ja025965s.

(39) Clayton Teague, E. Room Temperature Gold-Vacuum-Gold Tunneling Experiments. *J Res Natl Bur Stand (1934)* **1986**, *91* (4), 171–233. https://doi.org/10.6028/jres.091.027.

(40) Burzhuev, S.; Dâna, A.; Ortaç, B. Laser Synthesized Gold Nanoparticles for High Sensitive Strain Gauges. *Sensors and Actuators, A: Physical* **2013**, *203*, 131–136. https://doi.org/10.1016/J.SNA.2013.08.034.